ELSEVIER

Journal of Organometallic Chemistry 634 (2001) 61–68

Journal of Organometallic Chemistry

www.elsevier.com/locate/jorganchem

The metal–carbon stretching frequencies in methyl complexes of Rh, Ir, Ga and In with porphyrins and a tetradentate pyridine–amide ligand

Willetta Lai [a], Man-Kit Lau [a], Victor Chong [a], Wing-Tak Wong [b], Wa-Hung Leung [a,*], Nai-Teng Yu [a,*]

[a] *Department of Chemistry, The Hong Kong University of Science and Technology, Clear Water Bay, Kowloon, Hong Kong*
[b] *Department of Chemistry, The University of Hong Kong, Pokfulam Road, Hong Kong*

Received 4 May 2001; accepted 27 June 2001

Abstract

Interactions of *trans*-[Rh(bpb)(CH_3)(H_2O)] (**1**) [bpb = 1,2-bis(2-pyridinecarboxamido)benzene] with Lewis bases L afford the respective adducts *trans*-[Rh(bpb)(CH_3)(L)], where L = 4-substituted pyridine 4-Xpy (X = H (**2**), ^{t}Bu (**3**), NMe_2 (**4**) CN (**5**)), PMe_2Ph (**6**) or benzimidazole (**7**). The structures of complexes **3** and **6** have been established by X-ray crystallography. The Rh–C distance in complex **6** (2.095(6) Å) is longer than that in complex **3** (2.02(1) Å), indicating that PMe_2Ph has a stronger trans influence than 4-^{t}Bupy. The metal–carbon stretching frequencies for *trans*-[Rh(bpb)(CH_3)(L)] and [M(TTP)(CH_3)] [TTP = 5,10,15,20-tetrakis(4-methylphenyl)porphyrin dianion; M = Rh, Ir, Ga, In] have been determined by near IR FT-Raman spectroscopy. Complex **1** exhibits ν(Rh–C) at 562 cm^{-1}, which downshifts to 532 cm^{-1} upon deuteriation of the axial methyl group. Replacement of the aquo ligand in complex **1** with nitrogen ligands or phosphine resulted in downshift in ν(Rh–C). The ν(Rh–C) for *trans*-[Rh(bpb)(CH_3)(L)] was found to decrease in the order L: $PMe_2Ph \gg$ 4-Xpy ~ BzIm > H_2O, consistent the order of *trans* influence of L. For [M(TTP)(CH_3)] (M = Co, Rh, Ir, Ga, or In) the M–C force constant was found to decrease in the orders Ir > Rh > Co and Ga > In, consistent with the trends of metal–carbon bond strength for these metals. For *trans*-[Rh(bpb)(CH_3)(4-Xpy)] and *trans*-[Rh(TTP)(CH_3)(4-Xpy)], the ν(Rh–C) were found to be not very sensitive to the nature of X, suggesting that the electronic factors of the axial pyridine ligand do not have a significant effect on the Rh–C bonds for these rhodium alkyl complexes. © 2001 Published by Elsevier Science B.V.

Keywords: Metal methyl compounds; FT-Raman spectroscopy; Metal–carbon stretching frequency; *Trans* ligand effect

1. Introduction

Transition metal σ-alkyl compounds play central roles in organometallic [1] and bioinorganic [2] catalysis. A knowledge of factors affecting metal-carbon bond strength of transition metal alkyls may help elucidate mechanisms of organometallic reactions, and the better to understand the unique roles of certain metals in catalysis. Of special interest are cobalt(III) alkyls that are found in the active sites of two types of cobalamin, namely methylcobalamin and 5′-deoxyadenosylcobalamin, which mediate methyl group transfer and carbon skeletal rearrangement, respectively [3,4]. Since the breaking of the cobalt–alkyl bond is believed to be a key step in the catalytic cycles for these two types of cobalamin, efforts have been made to elucidate the factors affecting cobalt–alkyl bond strength for organocobalt(III) compounds [3,5]. In particular, Raman spectroscopy has proved to be a convenient technique to assess the ground-state properties of B_{12} and model compounds due to the correlation between the metal–carbon stretching frequency and

Abbreviations: Por, porphyrin dianion; TTP, 5,10,15,20-tetrakis(4-methylphenyl)porphyrin dianion; OEP, 2,3,7,8,12,13,17,18-octaethylporphyrin dianion; bpb, 1,2-bis(2-pyridinecarboxamido)benzene dianion; 4-Xpy, 4-X-substituted pyridine; BzIm, benzimidazole.

* Corresponding authors. Tel.: +852-2358-7360; fax: +852-2358-1594.

E-mail addresses: chleung@ust.hk (W.-H. Leung), chyu@ust.hk (N.-T. Yu).

0022-328X/01/$ - see front matter © 2001 Published by Elsevier Science B.V.
PII: S0022-328X(01)01097-X

metal–carbon bond dissociation energy. Using a near-infrared laser source for Raman excitation, which eliminates the problem of photolysis of light-sensitive cobalt alkyl compounds, the Co–C vibrational modes for methylcobalamins and model compounds have been unambiguously identified to be in the range of 500–515 cm^{-1} [6]. A similar stretching frequency was found for methylcobalamin by resonance Raman spectroscopy [7]. One issue that has attracted much attention is the role of the axial ligand in the Co–C bond activation for B_{12} coenzyme. The displacement of the axial benzimidazole group from the cobalt centre by a nitrogenous ligand was indicated by recent X-ray diffraction [8] and EPR [9] studies on methylmalonyl–CoA mutase. Although the axial base is known to accelerate the Co–C bond cleavage in B_{12} coenzyme [10], trans ligands were found to have little or no electronic effects on ν(Co–C) for both alkylcobaloximes [11] and alkylcobalamins [7,12]. In an effort to elucidate the factors governing metal–alkyl bond strength, and to address the question as to why cobalt is chosen as the metal centre for B_{12} chemistry, we set out to determine metal–carbon stretching frequencies for a series of metal methyl complexes by FT-Raman spectroscopy. Previously, we have reported on the stereoelectronic factors affecting Co–C stretching frequencies for cobalt(III) alkyls with a tetraaza chelate 1,2-bis(2-pyridinecarboxamido)benzene (H_2bpb) and porphyrins [6]. In this paper, we will extend our study to methyl complexes of other transition metals. The effects of metal substitution and axial base coordination on the metal–carbon stretching frequencies for *trans*-[Rh(bpb)(CH_3)(L)] (L = H_2O, 4-substituted pyridine, BzIm or PMe_2Ph) and [M(TTP)(CH_3)(L)] (M = Rh or Ir, L = 4-substituted pyridine) (Scheme 1) were examined. The crystal structures of *trans*-[Rh(bpb)(CH_3)(4-^{t}Bupy)] and *trans*-[Rh(bpb)(CH_3)(PMe_2Ph)] have been determined.

2. Experimental

2.1. General Information

Solvents were purified and distilled and degassed. All synthetic manipulations, unless otherwise stated, were carried out in air. NMR spectra were recorded on a Bruker ARX 300 spectrometer operating at 300 MHz, chemical shifts (δ/ ppm) were reported with reference to $SiMe_4$ (^{1}H) and H_3PO_4 (^{31}P).

The methyl complexes *trans*-[Rh(bpb)R(H_2O)] (R = CH_3 (**1**) or CD_3) were prepared according to the Che's procedure [13] by oxidative addition of Na[Rh(bpb)] with CH_3I or CD_3I, respectively, and purified by column chromatography (neutral alumina). The metalloporphyrins [Rh(por)(CH_3)] (por = TTP, OEP) [14], and [M(TTP)(CH_3)] (M = Ir [15], Ga [16], In [17]) were prepared according to the literature methods. The methyl-d_3 derivatives *trans*-[Rh(bpb)(CD_3)(H_2O)] and [Rh(por)(CD_3)] were prepared as for the corresponding methyl analogues using CD_3I instead of CH_3I, and [M(ttp)(CD_3)] prepared by methylation of [M(TTP)Cl] with CD_3MgI. The ^{1}H-NMR spectra for the methyl-d_3 complexes were found to be identical with those for the methyl analogues except that the axial methyl resonant signals were absent. ^{1}H-NMR spectral data for *trans*-[Rh(bpb)(CH_3)(L)] and *trans*-[M(bpb)(CH_3)(L)] (M = Rh, Ir) are collected in Section 5.

2.2. Preparations of trans-[Rh(bpb)(CH_3)(L)] (L = 4-Xpy where X = H (**2**), ^{t}Bu (**3**), NMe_2 (**4**), CN (**5**), PMe_2Ph (**6**), or BzIm (**7**))

Typically, to a solution of **1** (50 mg, 0.08 mmol) in MeOH (10 ml) an excess of L (ca. two equivalents) was added, and the mixture was stirred at room temperature (r.t.) for 30 min. Concentration (to ca. 5 cm^3) and

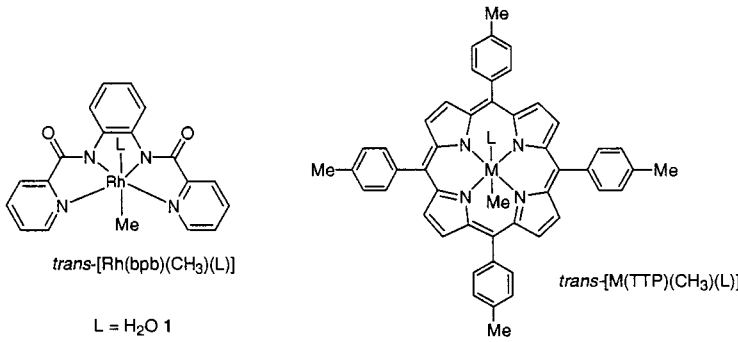

L = H_2O **1**
= py **2**
= 4-Bu^{t}py **3**
= 4-NMe_2py **4**
= 4-CNpy **5**
= PMe_2Ph **6**
= BzIm **7**

M = Rh
L = py **8**
= 4-Bu^{t}py **9**
= 4-NMe_2py **10**
= 4-CNpy **11**

M = Ir
L = py **12**
= 4-Bu^{t}py **13**
= 4-NMe_2py **14**
= 4-CNpy **15**

Scheme 1.

Table 1
Crystallographic data and experimental details for *trans*-[Rh(bpb)(CH_3)(4-Bu^{t}py)]·1/2Et_2O (**3**·1/2Et_2O) and *trans*-[Rh(bpb)(CH_3)(PMe_2Ph)]·1/2H_2O (**6**·1/2H_2O)

	3·1/2Et_2O	**6**·1/2H_2O
Empirical formula	$C_{30}H_{33}N_5O_{2.5}Rh$	$C_{27}H_{27}N_4O_{2.5}PRh$
Formula weight	606.53	581.41
Crystal color, habit	Orange, block	Orange, block
Crystal system	Triclinic	Monoclinic
Unit cell dimensions		
a (Å)	13.589(5)	15.987(3)
b (Å)	18.223(6)	16.481(4)
c (Å)	13.290(6)	19.418(2)
α (°)	110.85(3)	
β (°)	107.93(3)	98.97(1)
γ (°)	73.30(3)	
V (Å^3)	2866(2)	5053(1)
Space group	$P\bar{1}$ (no. 2)	$P2_1/a$ (no. 14)
Z	4	8
D_{calc} (g cm^{-3})	1.405	1.528
F(000)	1252	2376
μ (Mo–K_α) (cm^{-1})	6.31	7.72
T (K)	298.2	298.2
λ (Å)	0.71073	0.71073
Scan type	ω–2θ	ω–2θ
Total no. of reflections	7883	9589
Weighting scheme	$1/[\sigma^2(F_o) + 0.025F_o^2/4]$	$1/[\sigma^2(F_o) + 0.012F_o^2/4]$
No. of observations ($I>1.50\sigma(I)$)	4379	5967
$R(F)$	0.075	0.047
R_w	0.077	0.044
Goodness-of-fit (F)	1.71	1.37

addition of a large amount of Et_2O afforded an orange solid, which was collected, washed with MeOH, recrystallized from CH_2Cl_2–Et_2O, and characterized by ^{1}H-NMR spectroscopy [13] (yield 50–70%).

2.3. *trans*-[M(TTP)(CH_3)(4-Xpy)] (M = Rh, X = H (**8**), ^{t}Bu (**9**), NMe_2 (**10**), CN (**11**); M = Ir, X = H (**12**), ^{t}Bu (**13**), NMe_2 (**14**), CN (**15**))

Typically, to a solution of [M(TTP)(CH_3)] (50 mg, 0.08 mmol) in CH_2Cl_2 (10 cm^3) an excess of 4-Xpy (ca. two equivalents) was added. The mixture was stirred at r.t. for 30 min and was concentrated to ca. 5 cm^3. Addition of hexane (ca. 20 cm^3) and cooling to −10 °C afforded a purple solid, which was collected, washed with cold MeOH, and characterized by ^{1}H-NMR spectroscopy in $CDCl_3$ solution in the presence of 4X-py [18] (yield 60–70%).

2.4. FT-Raman measurements

FT-Raman data were acquired on a Bruker IFS 66/FRA FT-Raman spectrophotometer equipped with a highly sensitive Ge detector cooled by liquid nitrogen. The spectra were recorded via 180° scattering. The laser excitation used was 1.064 μm provided by a CW diode laser-pumped Nd: YAG laser. The number of scans taken was 50–200. The laser power employed was 50–100 mW (defocused) and the spectral resolution was 4.0 cm^{-1}. The samples were exposed to the laser beam in the solid form in an aluminum sample holder, which has a 2-mm hole driller at the centre.

2.5. X-ray crystallography

A summary of crystallographic data and experimental details for **3**·1/2Et_2O and **6**·1/2H_2O is shown in Table 1. All data were collected on a Rigaku AFC7R diffractometer using graphite-monochromated Mo–K_α radiation ($\lambda = 0.71073$ Å) at 25 °C. The structures were solved by direct methods. All data were corrected for Lorentz and polarization and absorption effects. The structures were refined on F by full matrix least-squares analyses. Hydrogen atoms were placed at the idealised positions (C–H = 0.95 Å). All calculations were performed using the TEXSAN [19] crystallographic software package.

3. Results

3.1. Syntheses of metal methyl complexes

The aquo ligands in *trans*-[Rh(bpb)(CH_3)(H_2O)] (**1**) was found to be labile and could be displaced readily by Lewis bases. Thus, the interaction of complex **1** with Lewis bases L afforded the corresponding adducts *trans*-[Rh(bpb)(CH_3)(L)] (L = 4-Xpy where X = H (**2**), ^{t}Bu (**3**), NMe_2 (**4**) and CN (**5**); PMe_2Ph (**6**) or BzIm (**7**)) that were characterized by ^{1}H-NMR spectroscopy. These adducts are stable in both the solid state and solution. Similarly, the six-coordinated pyridine adducts *trans*-[M(TTP)(CH_3)(4-Xpy)] (M = Rh, X = H (**8**), ^{t}Bu (**9**), NMe_2 (**10**), CN (**11**); Ir, X = H (**12**), ^{t}Bu (**13**), NMe_2 (**14**), CN (**15**)) were prepared from [M(TTP)(CH_3)] and 4-Xpy. The FT-Raman spectra of solid samples of complexes **8**–**15** showed that the M–C stretching modes were shifted with respect to those for [M(TTP)(CH_3)] (see later section), indicating that the 4-Xpy ligands are coordinated in these complexes.

3.2. Crystal structures of *trans*-[Rh(bpb)(CH_3)(L)] (L = 4-Bu^{t}py and PMe_2Ph)

The solid-state structures of **3** and **6** have been established by X-ray crystallography. For **3**, two independent molecules were found in the asymmetric unit. The structure of one of these molecules containing Rh(1) is shown in Fig. 1; selected bond lengths and angles are listed in Table 2. The geometry around Rh in

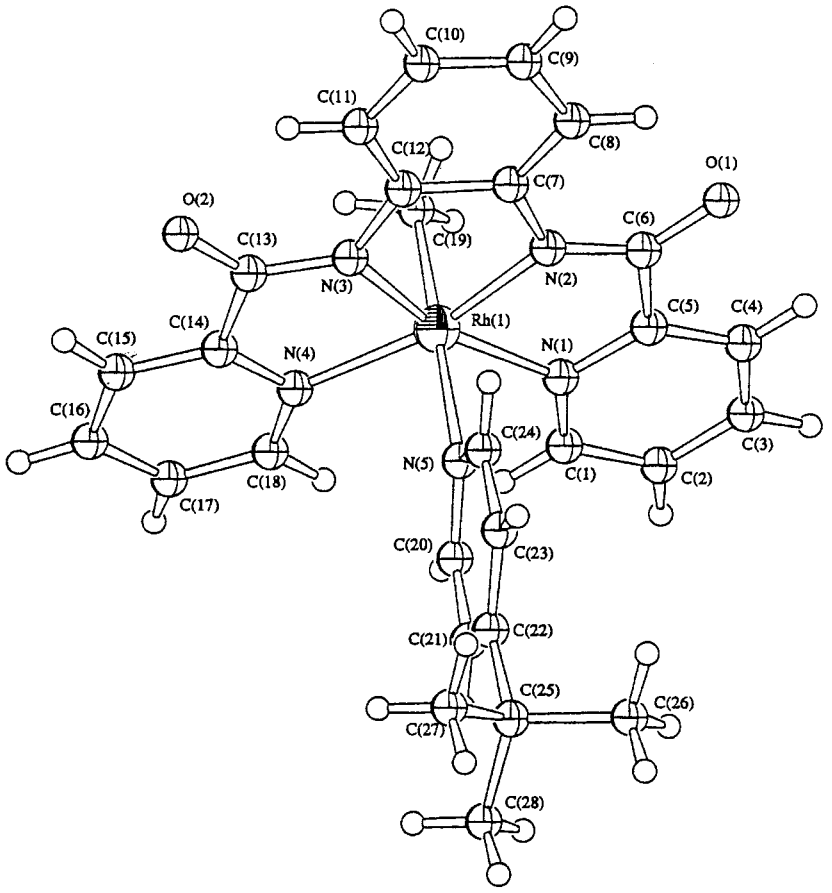

Fig. 1. Molecular structure of *trans*-[Rh(bpb)(CH_3)(4-^{t}Bupy)] (**3**).

3 is pseudo octahedral with the methyl group opposite to the 4-^{t}Bupy. The average Rh–N(bpb amide) (1.967 Å) and Rh–N(bpb pyridyl) (2.084 Å) are comparable to those for Na[Rh(bpb)Cl_2] [13]. The Rh–C bond distance (2.02(1) Å) is typical of octahedral rhodium(III) methyl complexes, e.g. 2.032(4) Å for [{Rh(TTP)(CH_3)}$_2$(μ-4-CNpy)] [20]. The Rh–N(4-^{t}Bupy) bond (2.203(10) Å) that is *trans* to the methyl group is considerably longer than the Rh–N(bpb pyridyl) bonds due to the *trans* influence of the methyl group. For complex **6**, the asymmetric unit also consists of two independent molecules. The structure of one of these molecules containing Rh(2) is shown in Fig. 2; selected bond lengths and angles are listed in Table 3. The geometry around Rh in complex **6** is pseudo octahedral with the methyl group opposite to the phosphine ligand. The Rh–C, Rh–P, average Rh–N(bpb amide) and average Rh–N(bpb pyridyl) distances are 2.095(6), 2.407(2), 1.980 and 2.096 Å, respectively. Despite the observed standard deviations, it is apparent that the average Rh–C bond distance in **6** is longer than that in **3**, indicating that the phosphine has a stronger *trans* influence than pyridine.

Table 2
Selected bond lengths (Å) and bond angles (°) for *trans*-[Rh(bpb)(CH_3)(4-^{t}Bupy)]·1/2Et_2O (**3**·1/2Et_2O)

Bond lengths			
Rh(1)–N(1)	2.082(9)	Rh(1)–N(2)	1.97(1)
Rh(1)–N(3)	1.965(9)	Rh(1)–N(4)	2.09(1)
Rh(1)–N(5)	2.203(9)	Rh(1)–C(19)	2.02(1)
Rh(2)–N(6)	2.10(1)	Rh(2)–N(7)	1.97(1)
Rh(2)–N(8)	1.977(10)	Rh(2)–N(9)	2.08(1)
Rh(2)–N(10)	2.22(1)	Rh(2)–C(47)	2.04(1)
Bond angles			
N(1)–Rh(1)–N(2)	80.8(4)	N(1)–Rh(1)–N(3)	164.1(5)
N(1)–Rh(1)–N(4)	114.8(4)	N(1)–Rh(1)–N(5)	90.0(4)
N(1)–Rh(1)–C(19)	89.4(5)	N(2)–Rh(1)–N(3)	83.4(5)
N(2)–Rh(1)–N(4)	164.1(4)	N(2)–Rh(1)–N(5)	92.5(4)
N(2)–Rh(1)–C(19)	88.3(6)	N(3)–Rh(1)–N(4)	80.9(4)
N(3)–Rh(1)–N(5)	92.0(4)	N(3)–Rh(1)–C(19)	88.8(4)
N(4)–Rh(1)–N(5)	90.7(4)	N(4)–Rh(1)–C(19)	88.8(6)
N(5)–Rh(1)–C(19)	179.0(5)	N(6)–Rh(2)–N(7)	80.0(4)
N(6)–Rh(2)–N(8)	164.0(5)	N(6)–Rh(2)–N(9)	115.3(4)
N(6)–Rh(2)–N(10)	93.5(4)	N(6)–Rh(2)–C(47)	88.6(5)
N(7)–Rh(2)–N(8)	84.1(4)	N(7)–Rh(2)–N(9)	164.0(4)
N(7)–Rh(2)–N(10)	93.3(4)	N(7)–Rh(2)–C(47)	88.7(5)
N(8)–Rh(2)–N(9)	80.4(4)	N(8)–Rh(2)–N(10)	89.5(4)
N(8)–Rh(2)–C(47)	88.9(5)	N(9)–Rh(2)–N(10)	90.3(4)
N(9)–Rh(2)–C(47)	87.3(5)	N(10)–Rh(2)–C(47)	177.3(6)

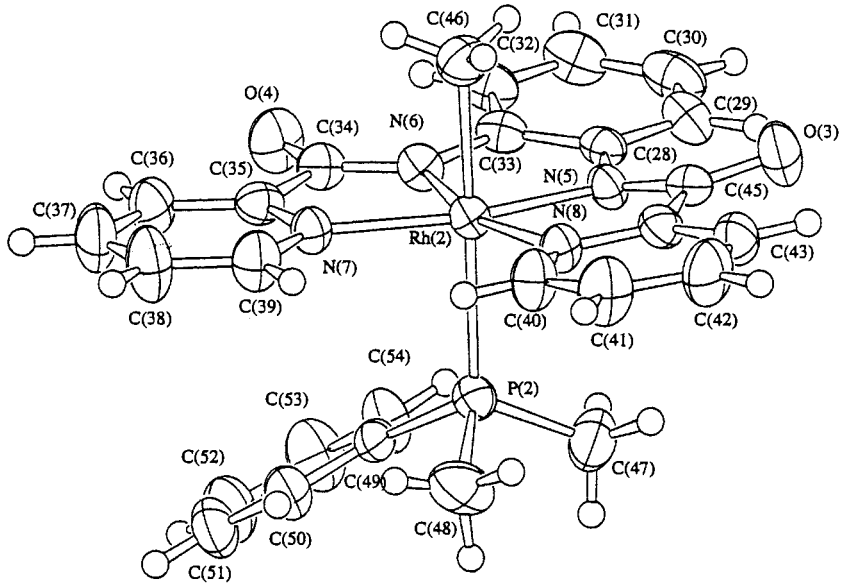

Fig. 2. Molecular structure of *trans*-[Rh(bpb)(CH_3)(PMe_2Ph)] (**6**).

3.3. Rh–C stretching frequencies for *trans*-[Rh(bpb)(CH_3)(L)]

The Rh–C stretching frequencies for *trans*-[Rh(bpb)(CH_3)(L)] (L = H_2O, 4-Xpy, BzIm, PMe_2Ph) in the solid state have been determined by FT-Raman spectroscopy and the results are summarized in Table 4. The Raman spectrum of compound **1** (Fig. 3a) shows a band at 562 cm^{-1}, which downshifts to 532 cm^{-1} upon deuteriation of the axial methyl group (Fig. 3b), is confidently assigned to ν(Rh–C). The observed isotope shift of 30 cm^{-1} is smaller than the theoretical value of 43 cm^{-1} probably due to coupling of ν(Rh–C) with some other vibrational modes of bpb. The ν(Rh–C) for complex **1** is higher than that for the cobalt congener *trans*-[Co(bpb)(CH_3)(H_2O)] (515 cm^{-1}) [6d]. Like *trans*-[Co(bpb)(CH_3)(H_2O)], replacement of the aquo ligand in complex **1** with 4-Xpy or BzIm resulted in lowering of ν(Rh–C). Although it appears that the electron-rich pyridine adducts (X = ^{t}Bu or NMe_2) have higher ν(Rh–C) than the less electron-rich ones, the electronic influence of the pyridine ligand on ν(Rh–C) is not big. The $\Delta\nu$(Rh–C) for *trans*-[Rh(bpb)(CH_3)(4-Xpy)], which is defined as the difference between ν(Rh–C) for the py adduct and that for the 4-Xpy adduct, is in the range of +4 to −6 cm^{-1}. A similar result was found for [Co($DH)_2$(CH_3)(4-Xpy)] (DH = dimethylglyoxime anion) which shows a $\Delta\nu$(Co–C) of ca. 10 cm^{-1} [6c]. The ν(Rh–C) for the PMe_2Ph adduct **6** is considerably lower than those for **1** and the pyridine adducts consistent with the strong *trans* influence of phosphine.

3.4. ν(M–C) for [M(TTP)(CH_3)(L)] (M = Rh, Ir, Ga or In)

The solid-state Raman ν(M–C) for metal methyl porphyrin complexes are listed in Table 5. [Rh(TTP)(CH_3)] exhibits a Raman-active band at 562 cm^{-1}, which shifts to 524 cm^{-1} upon deuteriation of the axial methyl group, is assigned as ν(Rh–C). Like

Table 3
Selected bond lengths (Å) and bond angles (°) for *trans*-[Rh(bpb)(CH_3)(PMe_2Ph)]·1/2H_2O (**6**·1/2H_2O)

Bond lengths			
Rh(1)–P(1)	2.413(2)	Rh(1)–N(1)	1.980(4)
Rh(1)–N(2)	1.974(5)	Rh(1)–N(3)	2.097(4)
Rh(1)–N(4)	2.074(5)	Rh(1)–C(19)	2.089(6)
Rh(2)–P(2)	2.407(2)	Rh(2)–N(5)	1.977(4)
Rh(2)–N(6)	1.982(5)	Rh(2)–N(7)	2.095(4)
Rh(2)–N(8)	2.096(5)	Rh(2)–C(46)	2.095(7)
Bond angles			
P(1)–Rh(1)–N(1)	91.4(1)	P(1)–Rh(1)–N(2)	90.6(1)
P(1)–Rh(1)–N(3)	89.5(1)	P(1)–Rh(1)–N(4)	93.3(1)
P(1)–Rh(1)–C(19)	178.9(2)	N(1)–Rh(1)–N(2)	84.6(2)
N(1)–Rh(1)–N(3)	165.1(2)	N(1)–Rh(1)–N(4)	80.5(2)
N(1)–Rh(1)–C(19)	89.5(2)	N(2)–Rh(1)–N(3)	80.5(2)
N(2)–Rh(1)–N(4)	164.6(2)	N(2)–Rh(1)–C(19)	88.9(2)
N(3)–Rh(1)–N(4)	114.4(2)	N(3)–Rh(1)–C(19)	89.5(2)
N(4)–Rh(1)–C(19)	87.4(2)	P(2)–Rh(2)–N(5)	93.9(1)
P(2)–Rh(2)–N(6)	93.8(1)	P(2)–Rh(2)–N(7)	88.8(1)
P(2)–Rh(2)–N(8)	91.5(1)	P(2)–Rh(2)–C(46)	177.3(2)
N(5)–Rh(2)–N(6)	84.3(2)	N(5)–Rh(2)–N(7)	164.3(2)
N(5)–Rh(2)–N(8)	79.7(2)	N(5)–Rh(2)–C(46)	88.2(2)
N(6)–Rh(2)–N(7)	80.1(2)	N(6)–Rh(2)–N(8)	163.4(2)
N(6)–Rh(2)–C(46)	88.1(2)	N(7)–Rh(2)–N(8)	115.7(2)
N(7)–Rh(2)–C(46)	89.7(2)	N(8)–Rh(2)–C(46)	87.1(2)

Table 4
Solid-state Rh–C stretching frequencies for *trans*-[Rh(bpb)(CH_3)(L)]

L	ν(Rh–C) (cm^{-1})	$\Delta\nu$(Rh–C) (cm^{-1}) [a]
H_2O	562	
H_2O	532 [b]	
py	556	0
4-^{t}Bupy	552	4
4-Me_2Npy	556	0
4-CNpy	562	−6
BzIm	555	
PMe_2Ph	514	

[a] $\Delta\nu$(Rh–C) = ν(Rh–C) for [Rh(bpb)(CH_3)(py)]–ν(Rh–C) for [Rh(bpb)(CH_3)(4-Xpy)].
[b] Methyl-d_3 complexes.

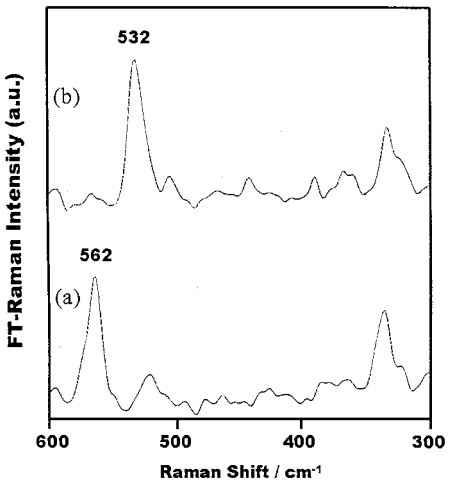

Fig. 3. FT-Raman spectra of *trans*-[Rh(bpb)R(H_2O)] in the solid state: R = CH_3 (a), CD_3 (b).

complex **1**, the observed isotope shift of 38 cm^{-1} for [Rh(TTP)(CH_3)] is smaller than the theoretical value. A slightly lower wavenumber (558 cm^{-1}) was found for the more basic OEP analogue [Rh(OEP)(CH_3)]. As might be expected, coordination of 4-Xpy to [Rh(ttp)(CH_3)] led to a downshift in ν(Rh–C), indicating that the Rh–C bonds in these octahedral adducts are weaker than that in square pyramidal [Rh(TTP)(CH_3)]. Like the Rh(bpb) system, the ν(Rh–C) for [Rh(TTP)(CH_3)(4-Xpy)] is not very sensitive to the electronic factors of 4-Xpy [$\Delta\nu$(Rh–C) $\leq$ 11 cm^{-1}]. [Ir(TTP)(CH_3)] exhibits ν(Ir–C) at 578 cm^{-1}, which is higher than those for [Co(TTP)(CH_3)] (503 cm^{-1}) and [Rh(TTP)(CH_3)]. Thus, for [M(TTP)(CH_3)], the M–C stretching frequency increases in the order Co < Rh < Ir. Again binding of 4-Xpy to [Ir(TTP)(CH_3)] results in a downshift in ν(Ir–C) with $\Delta\nu$(Ir–C) < 10 cm^{-1}. For [Ga(TTP)(CH_3)], the Raman-active band at 559 cm^{-1}, which shifts to 510 cm^{-1} upon deuteriation of the axial methyl group, is assigned to ν(Ga–C). By contrast to the rhodium and iridium analogues, the observed isotope shift of 49 cm^{-1} for [Ga(TTP)(CH_3)] is larger than the theoretical value (40 cm^{-1}). [In(TTP)(CH_3)] shows ν(In–C) at 501 cm^{-1} with an isotope shift of 44 cm^{-1}, which is also larger than the theoretical value. Thus, in contrast to the methyl complexes of cobalt triad, the metal–carbon stretching frequency for the Group 13 metal methyl complexes decreases down a group.

4. Discussion

4.1. Trends of M–C force constants for metal methyl complexes

In earlier studies, it was demonstrated that the cobalt–carbon force constant for organocobalt B_{12} model compounds correlates well with the Co–C bond strength [6]. The correlation of force constant with bond strength for cobalt alkyls is derived from the assumption that the Co–CH_3 moiety conforms to the Morse potential relationship, i.e. $U(r) = D_e\{1 - \exp[-a(r - r_e)]\}^2$ where $U(r)$ = potential energy, D_e = bond dissociation energy, r = bond length, r_e = equilibrium bond length, and a = constant. Under such a circumstance, the harmonic force constant (κ) of the Co–C bond is equal to the second derivative of $U(r)$ at $r = r_e$, i.e. $\kappa = 2D_e a^2$. Thus $\kappa/\kappa' = (D_e/D'_e)$.

If one assumes that the *iso*-structural metal methyl complexes [M(TTP)(CH_3)] have similar Morse potential characteristics, an analogous correlation of κ(M–C) with D_e(M–C) may also exist. Our Raman data for

Table 5
Solid-state M–C stretching frequencies for *trans*-[M(por)(CH_3)(L)]

M	por	L	ν(M–C) (cm^{-1})	$\Delta\nu$(Rh–C) (cm^{-1}) [a]
Co	TTP		503 [b]	
Rh	TTP		562	
Rh	TTP		524 [c]	
Rh	OEP		558	
Rh	OEP		526 [c]	
Rh	TTP	py	560	0
Rh	TTP	4-^{t}Bupy	549	11
Rh	TTP	4-NMe_2py	554	6
Rh	TTP	4-CNpy	563	−3
Rh	TTP	BzIm	563	
Ir	TTP		578	
Ir	TTP	py	577	0
Ir	TTP	4-^{t}Bupy	568	9
Ir	TTP	4-NMe_2py	571	6
Ir	TTP	4-CNpy	567	10
Ga	TTP		559	
Ga	TTP		510[c]	
In	TTP		501	
In	TTP		457[c]	

[a] $\Delta\nu$(M–C) = ν(M–C) for [M(TTP)(CH_3)(py)]–ν(M–C) for [M(TTP)(CH_3)(4-Xpy)].
[b] Ref. [6d].
[c] Methyl-d_3 complexes.

[M(TTP)(CH_3)] are indeed in line with such as correlation. For a diatomic oscillator M–CH_3, $\nu \propto (\kappa/\mu)^{1/2}$ or $\kappa \propto \nu^2\mu$ (where μ is the reduced mass of M and CH_3). Thus, for [M(TTP)(CH_3)] (M = Co, Rh, Ir), κ(Co–C): κ(Rh–C): κ(Ir–C) is calculated to be $(503)^2 \times 11.96$: $(563)^2 \times 13.11$: $(577)^2 \times 13.91 = 1$: 1.37: 1.53 (μ for Co–CH_3, Rh–CH_3 and Ir–CH_3 are 11.96, 13.11, and 13.91, respectively). The increasing order of M–C force constant is consistent with the trend that the M–C bond strength increases down a group for transition elements [21]. On the other hand, for [M(TTP)(CH_3)] (M = Ga, In), κ(Ga–C): κ(In–C) is calculated to be $(559)^2 \times 12.37$: $(501)^2 \times 13.29 = 1$: 0.863 (μ for Ga–CH_3 and In–CH_3 equal 12.37 and 13.29, respectively), which again is consistent with the trend of metal–carbon bond strength for main group elements [21].

4.2. Trans ligand effect on ν(M–C)

The ν(M–C) for *trans*-[Rh(bpb)(CH_3)(L)] (L = 4-Xpy and BzIm) are lower than those for **1**, suggesting that the N-donor ligands exhibit stronger trans influence than aquo. This finding is in contrast to the results for the methylcobalamin, for which the ν(Co–C) is independent of the displacement of the benzimidazole group [7]. Binding of 4-Xpy to [M(ttp)(CH_3)] (M = Rh, Ir) results in lowering in ν(M–C), indicating that the M–C bond is weakened by ligation of axial bases. It may be noted that the axial Co–C bond in [Co(OEP)(CH_3)(4-NMe_2py)] is longer than that in [Co(OEP)(CH_3)] by ca. 0.045 Å [22]. The ν(M–C) for *trans*-[Rh(bpb)(CH_3)(4-Xpy)] and [M(TTP)(CH_3)(4-Xpy)] are, however, not very sensitive to the nature of X. Therefore, like the previously studied alkylcobaloxime system [6], the electronic factors of 4-Xpy do not exhibit a significant influence on the ground-state properties of the M–C bond in both *trans*-[Rh(bpb)(CH_3)(4-Xpy)] and [M(TTP)(CH_3)(4-Xpy)]. It appears that the insensitivity of M–C force constant to nitrogen base coordination is quite common for alkyl complexes of transition metals, at least for the cobalt triads, and is apparently due to strong transition metal-to-alkyl covalent bonds. For B_{12} and model compounds, the strong covalent Co–C bond renders the opposite Co–N bond relatively weak regardless of the basicity of *trans* nitrogen ligands. Thus, coordination or displacement of axial nitrogen ligands to cobalt alkyls does not cause a significant change to the Co–C bond strength. Although for *trans*-[M(TTP)(CH_3)(4-Xpy)] (M = Rh, Ir) the M–N(py) bond is expected to be stronger than the Co–N counterpart, no electronic influence of 4-Xpy on M–C bond is observed because of the high M–C bond strength, as indicated by the large value of κ(M–C). On the other hand, phosphines such as PMe_2Ph exhibit strong *trans* influence to both rhodium and cobalt alkyls, as indicated by the low values of ν(M–C) for the phosphine adducts of these alkyls. X-ray crystallography revealed that the Rh–C bond in the phosphine adduct **6** is significantly longer than that in the pyridine adduct **3**. The strong *trans* influence of phosphine is attributed to the covalency of M–P bond and the ability of phosphines form π bonding with soft transition metals such as cobalt and rhodium.

4.3. Summary

In summary, the metal–carbon stretching modes for *trans*-[M(bpb)(CH_3)(L)] and *trans*-[M(bpb)(CH_3)(L)] have been determined by FT-Raman spectroscopy and assigned by deuterium-labeling experiments. Although a more sophisticated model of the metal–carbon vibrational mode, which includes the coupling of the metal–carbon stretches with other modes, is required in order to have a better agreement between the observed and theoretical isotope shifts, the conclusion of this paper does not rest on this. This work not only describes trends of metal–alkyl bond strengths but also gives some numerical values that allows a qualitative/semi-quantitative correlation between the metal–carbon stretching frequencies and the trans ligand and metal center effects. The conclusion is consistent with the X-ray data, and the well-known trans influence of ligands and trends of element-carbon bond strength: namely, for [M(TTP)(CH_3)], the M–C force constant decreases in the orders Ir > Rh > Co and Ga > In. For *trans*-[Rh(bpb)(CH_3)(4-Xpy)] and *trans*-[M(TTP)-(CH_3)(4-Xpy)] (M = Rh, Ir), the metal–carbon stretching frequencies are not sensitive to the electronic factors of pyridine ligand. It appears that the metal–carbon force constant for transition metal alkyls is rather insensitive to coordination of nitrogen ligands because of the strong *trans* influence of the alkyl group. Thus, the activation of B_{12} Co–C bond by enzyme is not due to weakening of the Co–C bond by the axial nitrogen bases. By contrast, phosphine ligands show a more pronounced *trans* influence on transition metal–alkyl bonds.

5. Supplementary material

Crystallographic data for the structural analysis have been deposited with the Cambridge Crystallographic Data Centre, CCDC Nos. 156615 for **3**·1/2Et_2O and 156616 for **6**·1/2H_2O. Copies of this information may be obtained free of charge from The Director, CCDC, 12 Union Road, Cambridge CB2 1EZ, UK (fax: +44-1233-336033; e-mail: deposit@ccdc.cam.ac.uk or www: http://www.ccdc.cam.ac.uk).

Acknowledgements

This work has been supported by the Research Grants Council of Hong Kong, China (project no. HKUST 6152/97P). We thank Tin-Ming Kwok for assistance in running FT-Raman spectra and Dr Zhenyang Lin for helpful discussions.

References

[1] R.H. Crabtree, Organometallic Chemistry of Transition Metals, Ch. 3, 2nd ed., Wiley, New York, 1987.
[2] H. Sigel, A. Sigel (Eds.), Metal Ions in Biological Systems, vol. 29, Marcel Dekker, New York, 1999.
[3] (a) L.G. Marzilli, in: J. Reedijik, E. Bouwman (Eds.), Bioinorganic Catalysis, Ch. 13, 2nd ed., Marcel Dekker, New York, 1993;
(b) L. Randaccio, Comment Inorg. Chem. 21 (1999) 327.
[4] D. Dolphin, B_{12}, Wiley, New York, 1982.
[5] (a) J. Halpern, Acc. Chem. Res. 15 (1982) 238;
(b) J. Halpern, Science 227 (1985) 869.
[6] (a) S. Nie, L.G. Marzilli, N.-T. Yu, J. Am. Chem. Soc. 111 (1989) 9526;
(b) S. Nie, P.A. Marzilli, L.G. Marzilli, N.-T. Yu, J. Chem. Soc. Chem. Commun. (1990) 770;
(c) S. Nie, P.A. Marzilli, L.G. Marzilli, N.-T. Yu, J. Am. Chem. Soc. 112 (1990) 6084;
(d) M. Chopra, T.S.M. Hun, W.-H. Leung, N.-T. Yu, Inorg. Chem. 34 (1995) 5973.
[7] S. Dong, R. Padmakumar, R. Banerjee, T.G. Spiro, J. Am. Chem. Soc. 118 (1996) 9182.
[8] C.L. Drenan, S. Huang, J.T. Drummond, R.G. Mathews, M.L. Ludwig, Science 266 (1994) 1669.
[9] R. Padmakumar, S. Taoka, R. Padmakumar, R. Banerjee, J. Am. Chem. Soc. 117 (1995) 7033.
[10] B.P. Hay, R.G. Finke, J. Am. Chem. Soc. 109 (1987) 8012.
[11] (a) J.M. Puckett Jr, M.B. Mitchell, S. Hirota, L.G. Marzilli, Inorg. Chem. 35 (1996) 4656;
(b) S. Hirota, S.M. Polson, J.M. Puckett Jr, S.J. Moore, M.B. Mitchell, L.G. Marzilli, Inorg. Chem. 35 (1996) 5646;
(c) S. Hirota, E. Kosugi, L.G. Marzilli, O. Yamauchi, Inorg. Chim. Acta 275–276 (1998) 90.
[12] (a) S. Dong, R. Padmakumar, N. Maiti, R. Banerjee, T.G. Spiro, J. Am. Chem. Soc. 120 (1998) 9947;
(b) S. Dong, R. Padmakumar, R. Banerjee, T.G. Spiro, Inorg. Chim. Acta 270 (1998) 392;
(c) S. Dong, R. Padmakumar, R. Banerjee, T.G. Spiro, J. Am. Chem. Soc. 121 (1999) 7063.
[13] S.-T. Mak, V.W.W. Yam, C.-M. Che, T.C.W. Mak, J. Chem. Soc. Dalton Trans. (1990) 2555.
[14] B.B. Wayland, S. Ba, A.E. Sherry, J. Am. Chem. Soc. 113 (1991) 530.
[15] H. Ogoshi, J.-I. Setsune, Z.-I. Yoshida, J. Organomet. Chem. 159 (1978) 317.
[16] A. Coutsolelos, R. Guilard, J. Organomet. Chem. 253 (1983) 273.
[17] R. Guilard, P. Cocolios, P. Fournari, J. Organomet. Chem. 129 (1977) C11.
[18] H. Ogoshi, J.-I. Setsune, T. Omura, Z.-I. Yoshida, J. Am. Chem. Soc. 97 (1975) 6461.
[19] TEXSAN: Crystal Structure Analysis Package, Molecular Structure Corporation, 1985 and 1992.
[20] W.-H. Leung, W. Lai, I.D. Williams, J. Organomet. Chem. 604 (2000) 197.
[21] A. Yamamoto, Organotransition Metal Chemistry, Wiley, New York, 1986, p. 42.
[22] J.S. Summers, J.L. Petersen, A.M. Stolzenberg, J. Am. Chem. Soc. 116 (1994) 7189.